Supplemental information for:

Poly (ADP-ribose) polymerase-1 is a key mediator of liver inflammation and fibrosis

Short Title: PARP-1 in liver inflammation and fibrosis

Partha Mukhopadhyay[1*], Mohanraj Rajesh[1*], Zongxian Cao[1*], Béla Horváth[1,2*], Ogyi Park[3*], Hua Wang[3], Katalin Erdélyi[1], Eileen Holovac[1], Yuping Wang[1], Lucas Liaudet[4], Nabila Hamdaoui[5,6], Fouad Lafdil[5,6], György Haskó[7], Csaba Szabo[8], A. Hamid Boulares[9], Bin Gao[3] and Pal Pacher[1]

Affiliations:

[1]Laboratory of Physiological Studies, National Institutes of Health/NIAAA, Bethesda, MD, USA.

[2]Pathology and Laboratory Medicine Institute, Cleveland Clinic, Cleveland, Ohio, USA.

[3]Laboratory of Liver Biology, National Institutes of Health/NIAAA, Bethesda, MD, USA.

[4]Department of Intensive Care Medicine, BH 08-621-University Hospital Medical, Center, 1011 LAUSANNE, Switzerland.

[5]Institut National de la Santé et de la Recherche Médicale (INSERM), U955, Créteil, F-94000 France.

[6]Université Paris-Est, Faculté de Médecine, UMR-S955, Créteil, F-94000 France.

[7]Departments of Surgery Rutgers New Jersey Medical School, Newark, New Jersey, USA.

[8]Department of Anesthesiology, University of Texas Medical Branch, Galveston, TX, USA.

[9]The Stanley Scott Cancer Center and Department of Pharmacology, Louisiana State University Health Sciences Center, New Orleans, LA 70112, USA

*equally contributed to this work. Correspondence to: pacher@mail.nih.gov

Detailed Materials and Methods

Hepatic tissue samples from human subjects

Alcoholic and hepatitis B virus-associated cirrhotic liver samples (stage 3-4 fibrosis) were collected from donor livers during liver transplantation from the Liver Tissue Cell Distribution System (LTCDS), University of Minnesota. Subjects with alcoholic cirrhosis (1 female (56 years old), and 5 males (60, 56, 48, 50, and 45 years old) were consuming more than 50g/day alcohol for at least 4-5 years. Among HBV-induced cirrhotic subjects 1 was female (46 years old) and 5 were males (45, 43, 40, 48, and 48 years old). The samples were collected by quick freezing in liquid nitrogen, and diagnosed by histological analysis. Normal healthy liver samples (3 females (32, 57, and 34 years old), and 3 males (56, 55, and 56 years old)) were also provided by the LTCDS, and represent the part of healthy donor livers that was not used for transplantation.

Induction of liver injury by CCl_4 and treatments

For the induction of acute liver injury by CCl_4 , mice were injected intraperitoneally (I.P) with a single dose of CCl_4 (10 % in olive oil (Sigma chemicals), 2 mL/kg) and sacrificed after 48 hrs. Chronic liver injury was instituted with CCl_4 (10 % in olive oil (Sigma chemicals), 2 mL/kg, 3 times/week) by intraperitoneal injections for 4 weeks (1). The PARP inhibitors (5-aminoisoquinolinone-hydrochloride (termed AIQ) and N-(-oxo-5,6-dihydro-phenanthridin-2-yl)-N,N-dimethylacetamide (PJ34) were obtained from Enzo Life Sciences and Sigma Chemicals, respectively). Mice were treated with the PARP inhibitors at 10 mg/kg/day i.p. In a separate set of experiments, mice were injected with CCl_4 alone for 4 weeks, and then treated with PARP inhibitors (10 mg/kg/day) or vehicle in the presence of CCl_4 for an additional 4 weeks. The respective control groups were treated with vehicle (2 mL/kg olive oil). After the treatments, mice were sacrificed, livers were excised and were frozen in liquid nitrogen or fixed in 10% neutral buffered formalin for biochemical and histological evaluations respectively. All the animals were provided with food and water *ad libitum.*

Induction of liver fibrosis by bile duct ligation (BDL)

Mice were anesthetized by intraperitoneal injection of ketamine (100 mg/kg) and xylazine (10 mg/kg). The abdomen was opened by a midline laparotomy and the common bile duct was identified and carefully separated from the surrounding connective tissue and hepatic artery and portal vein. The common bile duct was ligated with 5-0 silk thread at two locations close to the beginning of its intrapancreatic portion and was transected between the two ligatures. The

gallbladder was not removed. In sham-operated control, the common bile duct was identified but not ligated or transected. The incision was closed with metal clips. The mice were sacrificed two weeks after the surgery (2). To test the effect of PARP inhibition on BDL-induced hepatic fibrosis, mice received one dose of pre-operative IP injection of PJ34 or AIQ and daily post-operative IP injection of the inhibitors (10mg/kg/day) for two weeks.

Determination of liver function

On the day of the sacrifice, blood was collected and serum was prepared immediately followed by the determination of the serum levels of alanine aminotransferase (ALT) using a clinical chemistry analyzer - Idexx VetTest 8008 (Idexx Laboratories, Westbrook, ME, USA) (3, 4)

Histology and immunohistochemistry

After routine processing paraffin liver sections (5μm) were staining with hematoxylin and eosin (H&E) for histological evaluation of liver injury by CCl_4 (3). Immunostaining for α smooth muscle actin (α-SMA) was performed on paraffin sections using α-SMA antibody (clone 1A4, Dako, Carpinteria, CA) and developed using a biotinylated alkaline phosphatase-conjugated secondary antibody and DAB substrate kits from Vector laboratories.

Picro-Sirius Red staining, quantitative analysis of hepatic fibrosis

The mouse live tissue samples were fixed in 10% buffered formalin and then embedded in paraffin for sectioning. Hepatic fibrosis was analyzed by Picro-Sirius Red staining according to standard methods in routine pathology. The amount of collagen deposition was quantified by measuring the proportion of Sirius Red-stained area using color thresholding and measurement of area fraction with IMAGEJ software (NIH Public Domain). Images taken from 10 random 100× fields from the liver lobe of each animal were measured (n=4-7 animals/group).

Oil Red O staining for hepatic lipid accumulation

Liver samples embedded in optimal cutting temperature (*OCT*) compound were cut at 10 μM sections and stained with Oil Red O to evaluate the hepatic lipid content. Briefly, cryosections were air dried and fixed in 10% formalin and then stained with 0.5% Oil Red O in propylene glycol for 10 min at 60°C and subsequently washed with 85% propylene glycol. Sections were counterstained with hematoxylin, washed in water and mounted with aqueous solution.

Determination of hepatic triglyceride content

Triglyceride content was measured from liver tissue by Triglyceride Quantification Colorimetric Kit (Biovision) according to manufacturer's instruction.

Determination of PARP activity

PARP activities in the hepatic tissue homogenates were performed using the colorimetric assay kit (Trevigen Inc., Gaithersburg, MD). In brief, the assay was based on determining the biotinylated poly (ADP-ribose) incorporation on to the histone proteins coated in ELISA wells. Each sample was run in duplicate and the values were expressed as units/mg protein (4, 5)

Reverse Transcription and real time PCR

Hepatic tissues were homogenized and total RNA was isolated using Trizol LS reagent (Invitrogen) according to manufacturer's instruction. The RNA was treated with RNase-free DNase (Ambion, TX) to remove traces of genomic DNA contamination. Total RNA was then reverse-transcribed to cDNA using the Super-Script II (Invitrogen) and the target genes were amplified using the standard real time PCR kit (Applied Biosystems, Foster city CA). The amplification was performed in real time PCR system (Applied Biosystems, CA) using the following conditions: initial denaturation at 95 °C for 2 min, followed by 35 cycles were performed at 95 °C for 30 s and 60 °C for 30s. Primers used for amplification were reported by us or others earlier (4-8) and are provided in Supplemental Tables 1 and 2.

Western immunoblot analysis

Hepatic tissues were homogenized in mammalian tissue protein extraction reagent (TPER, Pierce Biotechnology, IL) supplemented with protease and phosphatase inhibitors (Roche, GmbH). Then samples were kept on ice for 1 hr, followed by centrifugation at 13,000 rpm for 30 min at 4°C. The supernatants were carefully collected and protein content was determined using Lowry assay kit (Bio-Rad, CA). 30 µg of protein was resolved in 12% SDS-PAGE and transferred to nitrocellulose membranes (GE Healthcare). Blocking was performed for 2 hr at room temperature with 5% non-fat skimmed milk powder prepared in PBS containing 0.1% tween 20 (Sigma). After washing with PBST, membranes were probed with either mouse monoclonal α-SMA (Sigma chemicals or Abcam) or rabbit polyclonal anti-poly(ADP ribose)/ PAR antibody (BDBiosciences, or Trevigen) or Collagen 1 (Abcam) and were used at 1:1000 dilution over night at 4°C. After subsequent washing with PBST, the membrane was incubated with secondary antibody - antimouse/ rabbit HRP (Applied bio systems) at RT for 1 hr. Then the membranes were developed using chemiluminescence detection kit (Super signal -west pico substrate,

Pierce). To confirm uniform loading, membranes were stripped and re-probed with β- actin (Chemicon, CA) or GAPDH (Abcam)

Determination of mitochondrial complex activities

Microplate assay kits (Abcam) were used to determine the activity of mitochondrial complex I, complex II, and complex IV according to the manufacturer's instructions. The complex enzymes were immunocaptured and activities were measured kinetics. Activities were calculated based on the manufacterur's instruction. Complex activities were expressed as fold change compared to the liver samples of the vehicle-treated mice as described (4).

Mitochondrial DNA content:

Mitochondrial DNA (mtDNA) determination was performed as previously described (7, 8) and the primers are provided in Supplemental Tables 1 and 2.

Hepatic 4-hydroxynonenal (4-HNE) content

Levels of hepatic 4-HNE were measured by using the kit procured from (Cell Biolabs, San Diego, CA, USA). In brief, BSA or hepatic tissue homogenates (10µg/ml) were absorbed on to the 96-well plates for 12h at 4ºC. The HNE adducts contained in the samples were captured with anti 4-HNE antibody, followed by a HRP-conjugated secondary antibody. The 4-HNE in the samples was determined based on standard curve generated with BSA-HNE as per the protocol supplied by the manufacturer (4).

Hepatic protein 3-nitrotyrosine (3-NT) content

Hepatic 3-NT levels were determined with ELISA kit from Hycult biotechnology, Cell sciences, Canton, MA, USA, as described earlier (4).

Myeloperoxidase (MPO) activity

MPO activities in the hepatic tissues were determined by fluorometric kit (Enzo life sciences, Plymouth Meeting, PA, USA). In brief the MPO in the samples oxidizes the non-fluorescent substrate in the presence of hydrogen peroxide to yield the fluorescent analog, which was measured at 590-600 nm emission wavelengths. The standard curve was plotted with recombinant MPO supplied with the kit (4, 5).

Determination of hepatic hydroxyproline content

The levels of hepatic hydroxyproline content in the tissue hydrolysates, a direct measure of the collagen content, were determined by the kit obtained from (BioVision, Mountain View, CA). In brief, 50 mg of hepatic tissue was homogenized in 500 µl of dH_2O and to this 200 µl of concentrated HCl (12N) was added and hydrolyzed at 110 ºC for 4 hrs. Then 10 µl of the hydrolysates were evaporated to dryness under vacuum and to this 100 µl of chloramine T reagent was added and incubated for 5 min. in the subsequent step 100 µl Ehrlich's reagent (dimethyl amino benzaldehyde) was added and incubated for 90 minutes at 60 ºC, then samples/standards were transferred to 96 well plates and absorbance was measured at 560 nm. The hydroxyproline content in the tissue hydrolysates was determined from the standard curve of 4-hydroxy-L-proline as per the instructions supplied by the vendor.

Isolation and culture of mouse hepatocytes and hepatic stellate cells

Primary mouse hepatocytes were isolated as described earlier (3). Mouse liver hepatic stellate cells (HSC) were isolated by in situ collagenase perfusion and differential centrifugation on OptiPrep density gradients. After perfusion of the liver of the deeply anesthetized mice, the livers were excised and the HSL cells were isolated(3, 9).

Determination of hepatocyte apoptosis/cell death by flow cytometer

Mice primary hepatocytes were treated with hydrogen peroxide (H_2O_2, 3mmol/L) in the presence or absence of PARP inhibitors (AIQ and PJ34 - 3mmol/L each) for 16h and apoptosis/cell death was determined with flow cytometry. Annexin V-APC was used as early apoptosis marker whereas Sytox Green was used as cell necrosis marker as described earlier (10).

Activation of hepatic stellate cells (HSC)

Isolated HSC were plated on to 96 well plates and maintained with RPMI 1640 medium with 10% FBS and supplemented antibiotic/antimycotic agents for 24 hrs or 7 days in the presence or absence of PARP inhibitors (AIQ and PJ34 10 mmol/L each). In a separate set of experiments $PARP^{+/+}$ and $PARP^{-/-}$ cells were compared under similar conditions (1 and 7 days). The effects of PARP inhibition or genetic deletion of PARP1 on HSC activation markers were determined by the mRNA/protein expression of a-SMA, collagen-1, and other pro-fibrotic markers described in the corresponding results sections and figures.

Supplemental Figure legends

Suppl. Fig.1. Acute CCl_4 treatment induces time-dependent liver injury and PARP activation. In this set of acute experiments, mice were treated with a single high dose of CCl_4 I.P. as described in methods. (A) Shows the time-dependen changes in serum ALT activities following a single high dose of CCL_4 injection. (B and C) Demonstrates alterations in oxidative/nitrative stress markers such as (B) 3-NT and (C) 4-HNE, respectively. (D) Shows time-dependent alterations of PARP activities in the hepatic tissues and (E) representative immunoblot with two different anti-PAR antibodies (Trevigen and BD) depicting the poly(ADP)ribosylated proteins. n=8-10/group for A-D; P* <0.05 vs. vehicle.

Suppl. Fig. 2. Deficiency of $PARP1^{-/-}$ attenuates the CCl_4 -induced acute liver injury and inflammation. For these experiments liver tissues were collected 48 hours following a single high dose of I.P. CCl_4 injection as described in methods. (A) Shows the representative images of hematoxylin-eosin (H&E) stained paraffin liver sections from the groups as indicated. The scale depicts 100mm. (B) Shows the serum ALT levels in the respective groups. (C) Depicts myeloperoxidase (MPO) activities in the hepatic tissues and (D) shows the mRNA expression of pro-inflammatory cytokines (TNF-a, IL1-b) and chemokines (MIP1-a, MIP2, MCP-1) n=8/group, *P<0.05 vs. $PARP^{+/+}$/$PARP1^{-/-}$ mice treated with vehicle. #P< 0.05 vs. $PARP^{+/+}$+CCl_4.

Suppl. Fig. 3. Pharmacological inhibition of PARP ameliorates CCl_4-induced acute liver injury and inflammation. For these experiments liver tissues were collected 48 hours following a single high dose of I.P. CCl_4 injection as described in methods. A) Representative H&E images from the respective groups are shown. The scale depicts 100mm. (B) Shows the serum ALT levels, n=6-12/group, *P< 0.05 vs. vehicle/PJ34/AIQ alone; #P < 0.05 vs. CCl_4 + PJ34/AIQ. (C) shows the mRNA expression of pro-inflammatory cytokines (TNF-a, IL1-b) and chemokines (MIP1-a, MIP2, MCP-1) from the hepatic tissues, n=8/group, *P< 0.05 vs. vehicle/PJ34/AIQ alone; #P< 0.05 vs. CCl_4 + PJ34/AIQ.

Suppl. Fig. 4. Genetic ablation* or *pharmacological inhibition* of *PARP attenuates chronic CCl_4 -treatment induced stellate cell activation in vivo

For these experiments liver tissues were collected 4 weeks following multiple CCl_4 injection as described in the methods. Part (A) shows representative images of paraffin embedded liver sections stained with α-SMA, a marker for HSC activation, in $PARP^{+/+}$/$PARP\text{-}1^{-/-}$ mice treated with vehicle or CCl_4 for 4 weeks, and the quantification of the staining right. Part (B) shows representative images of α-SMA staining in mice treated with vehicle, PARP inhibitors alone, or their combination with CCl_4, and the quantification of the staining right. The scale depicts 100mm in panels A and B. n=8/group, *P<0.05 vehicle vs. CCl_4 in $PARP^{+/+}$/$PARP\text{-}1^{-/-}$ mice (A) or vehicle/PJ34/AIQ alone vs. CCl_4 (B); #P<0.05 CCl_4 in $PARP^{+/+}$ vs. $PARP\text{-}1^{-/-}$ mice (A) or CCl_4 vs. CCl_4+PJ34/AIQ in WT mice (B).

Suppl. Fig. 5. Pharmacological inhibition of PARP attenuates the established stellate cell activation. After reaching 4 weeks of CCl_4 or vehicle treatment mice continued to receive CCl_4, vehicle, PARP inhibitors alone or PARP inhibitors in combination with CCl_4 for additional 4 weeks. Representative liver sections stained for α-SMA expression and its quantification. n=8/group, *P<0.05 vs. vehicle/PJ34/AIQ alone; #P< 0.05 CCl_4 vs. CCl_4 + PJ34/AIQ.

Suppl. Fig. 6. Pharmacological inhibition of PARP or chronic CCl_4 exposure or their combination does not alter liver fat content.

Part (A) shows representative liver sections stained with Oil Red O and light hematoxylin of mice treated with vehicle, CCl_4 or CCl_4+PJ34/AIQ. Please note absence of positive (red) Oil Red O staining, indicating absence of significant lipid accumulation in these liver sections. In contrast, the positive control liver sections from an alcohol-induced steatohepatitis model show nice positive staining. Part (B) shows quantification of hepatic triglyceride content in livers, which is essentially similar to the results described in part A. n=8/group, *P<0.05 vs. vehicle.

Supplemental References

1. Park O, Jeong W-IL, Wang L, Wang H, Lian Z-X, Gershwin ME, Gao B. Diverse roles of invariant natural killer T cells in liver injury and fibrosis induced by carbon tetrachloride. Hepatology 2009;49:1683-1694.

2. Guillot A, Hamdaoui N, Bizy A, Zoltani K, Souktani R, Zafrani ES, Mallat A, et al. Cannabinoid receptor 2 counteracts interleukin-17-induced immune and fibrogenic responses in mouse liver. Hepatology 2013 in press.

3. Cao Z, Mulvihill MM, Mukhopadhyay P, Xu H, Erdelyi K, Hao E, Holovac E, et al. Monoacylglycerol lipase controls endocannabinoid and eicosanoid signaling and hepatic injury in mice. Gastroenterology 2013;144:808-817.

4. Mukhopadhyay P, Horvath B, Zsengeller Z, Batkai S, Cao Z, Kechrid M, Holovac E, et al. Mitochondrial reactive oxygen species generation triggers inflammatory response and tissue injury associated with hepatic ischemia-reperfusion: therapeutic potential of mitochondrially targeted antioxidants. Free radical biology & medicine 2012;53:1123-1138.

5. Mukhopadhyay P, Rajesh M, Horváth B, Bátkai S, Park O, Tanchian G, Gao RY, et al. Cannabidiol protects against hepatic ischemia/reperfusion injury by attenuating inflammatory signaling and response, oxidative/nitrative stress, and cell death. Free Radical Biology and Medicine 2011;50:1368-1381.

6. Rajesh M, Mukhopadhyay P, Batkai S, Patel V, Saito K, Matsumoto S, Kashiwaya Y, et al. Cannabidiol attenuates cardiac dysfunction, oxidative stress, fibrosis, and inflammatory and cell death signaling pathways in diabetic cardiomyopathy. Journal of the American College of Cardiology 2010;56:2115-2125.

7. Bai P, Canto C, Oudart H, Brunyanszki A, Cen Y, Thomas C, Yamamoto H, et al. PARP-1 inhibition increases mitochondrial metabolism through SIRT1 activation. Cell Metabolism 2011;13:461-468.

8. Bai P, Canto C, Brunyanszki A, Huber A, Szanto M, Cen Y, Yamamoto H, et al. PARP-2 regulates SIRT1 expression and whole-body energy expenditure. Cell Metabolism 2011;13:450-460.

9. Jeong WI, Park O, Radaeva S, Gao B. STAT1 inhibits liver fibrosis in mice by inhibiting stellate cell proliferation and stimulating NK cell cytotoxicity. Hepatology 2006;44:1441-1451.

10. Mukhopadhyay P, Rajesh M, Hasko G, Hawkins BJ, Madesh M, Pacher P. Simultaneous detection of apoptosis and mitochondrial superoxide production in live cells by flow cytometry and confocal microscopy. Nature Protocols 2007;2:2295-2301.

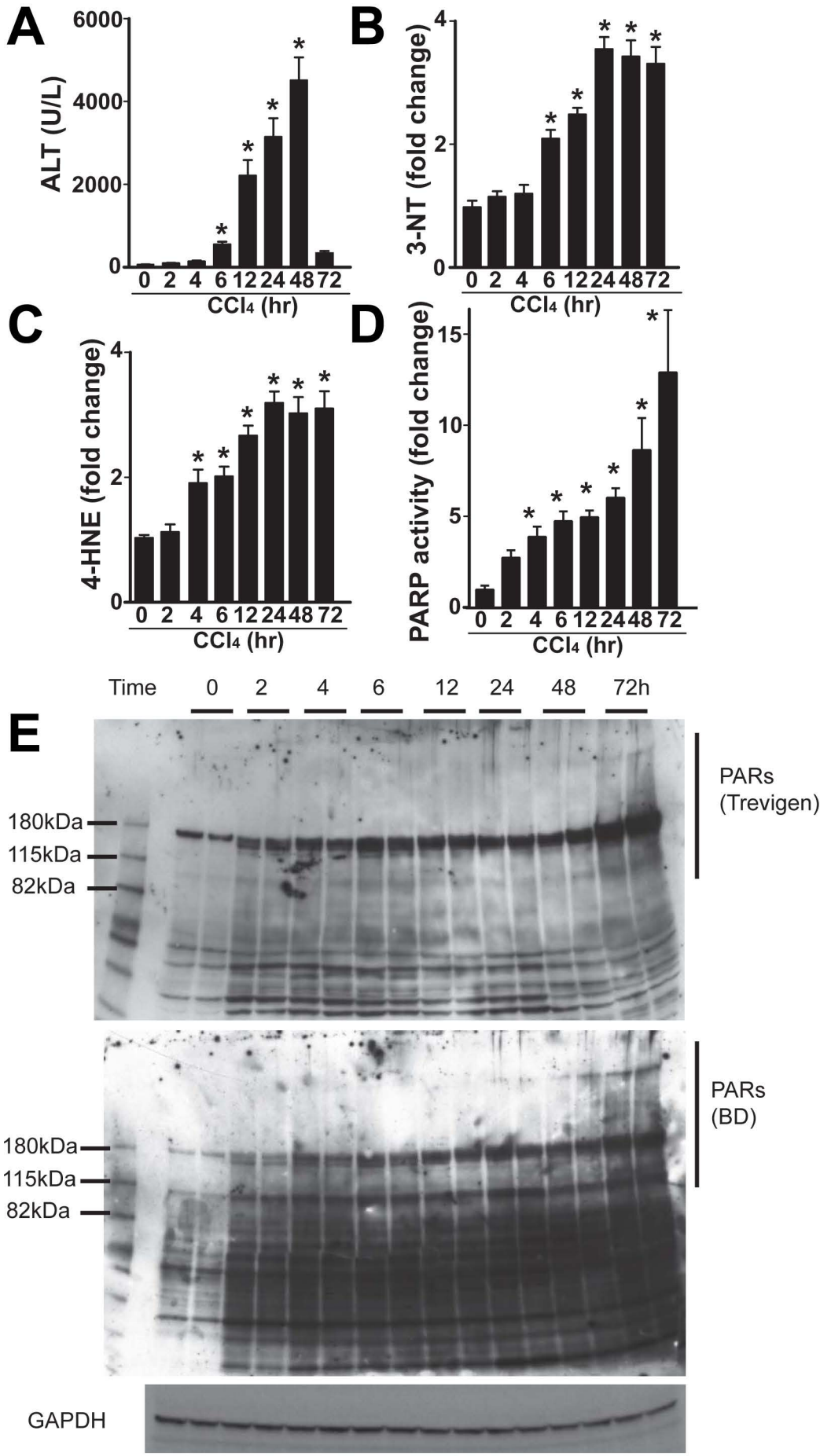
A
ALT (U/L)
6000
4000
2000
0
0 2 4 6 12 24 48 72
CCl4 (hr)
B
3-NT (fold change)
4
2
0
0 2 4 6 12 24 48 72
CCl4 (hr)
C
4-HNE (fold change)
4
2
0
0 2 4 6 12 24 48 72
CCl4 (hr)
D
PARP activity (fold change)
15
10
5
0
0 2 4 6 12 24 48 72
CCl4 (hr)
Time 0 2 4 6 12 24 48 72h
E
180kDa
115kDa
82kDa
PARs (Trevigen)
180kDa
115kDa
82kDa
PARs (BD)
GAPDH

Suppl. Fig. 1

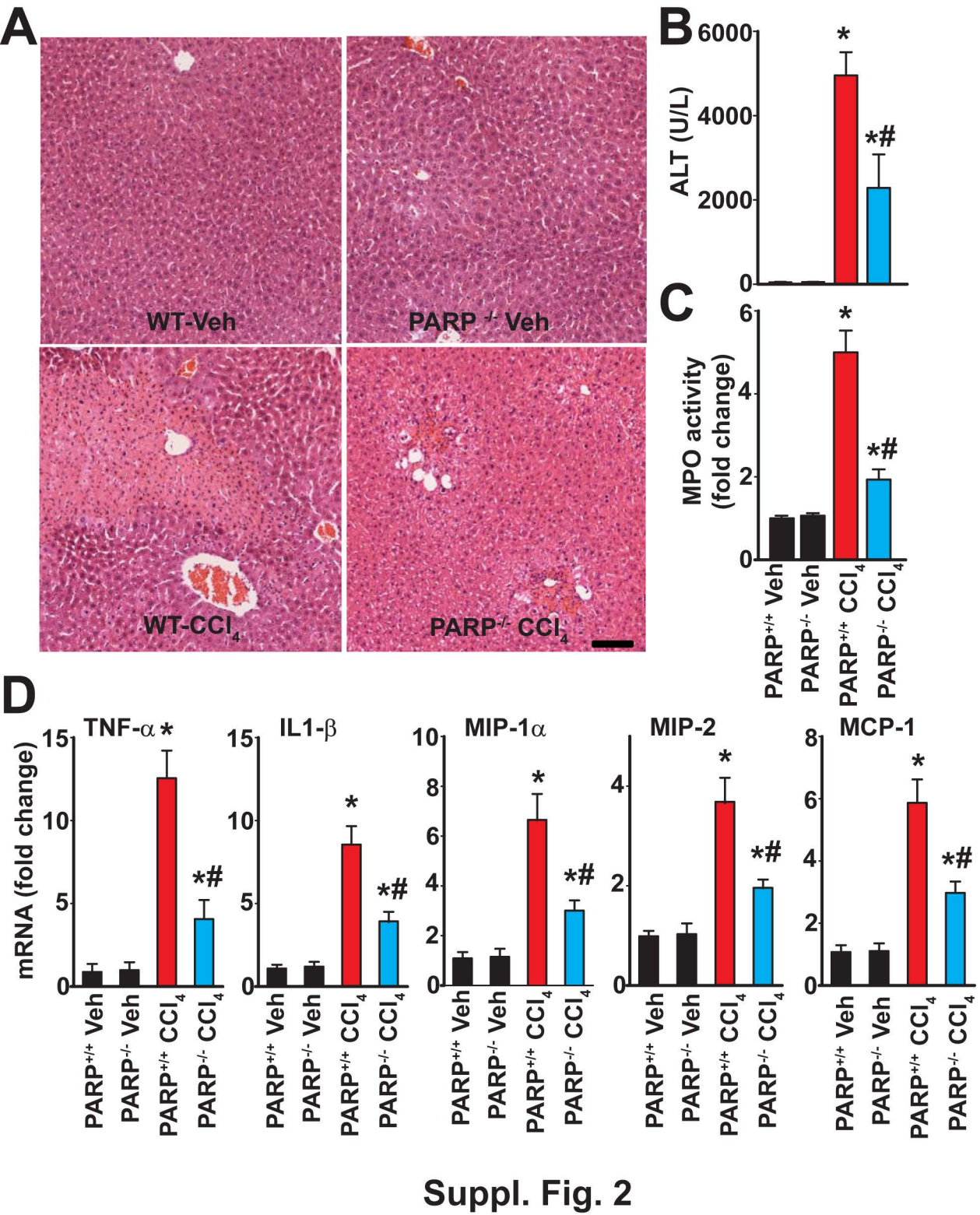
A
WT-Veh
PARP -/- Veh
WT-CCl4
PARP-/- CCl4
B
ALT (U/L)
6000
4000
2000
0
*
*#
C
MPO activity (fold change)
6
4
2
0
*
*#
PARP+/+ Veh
PARP-/- Veh
PARP+/+ CCl4
PARP-/- CCl4
D
mRNA (fold change)
TNF-α *
IL1-β
MIP-1α
MIP-2
MCP-1
15
10
5
0
8
6
4
2
*
*#

Suppl. Fig. 2

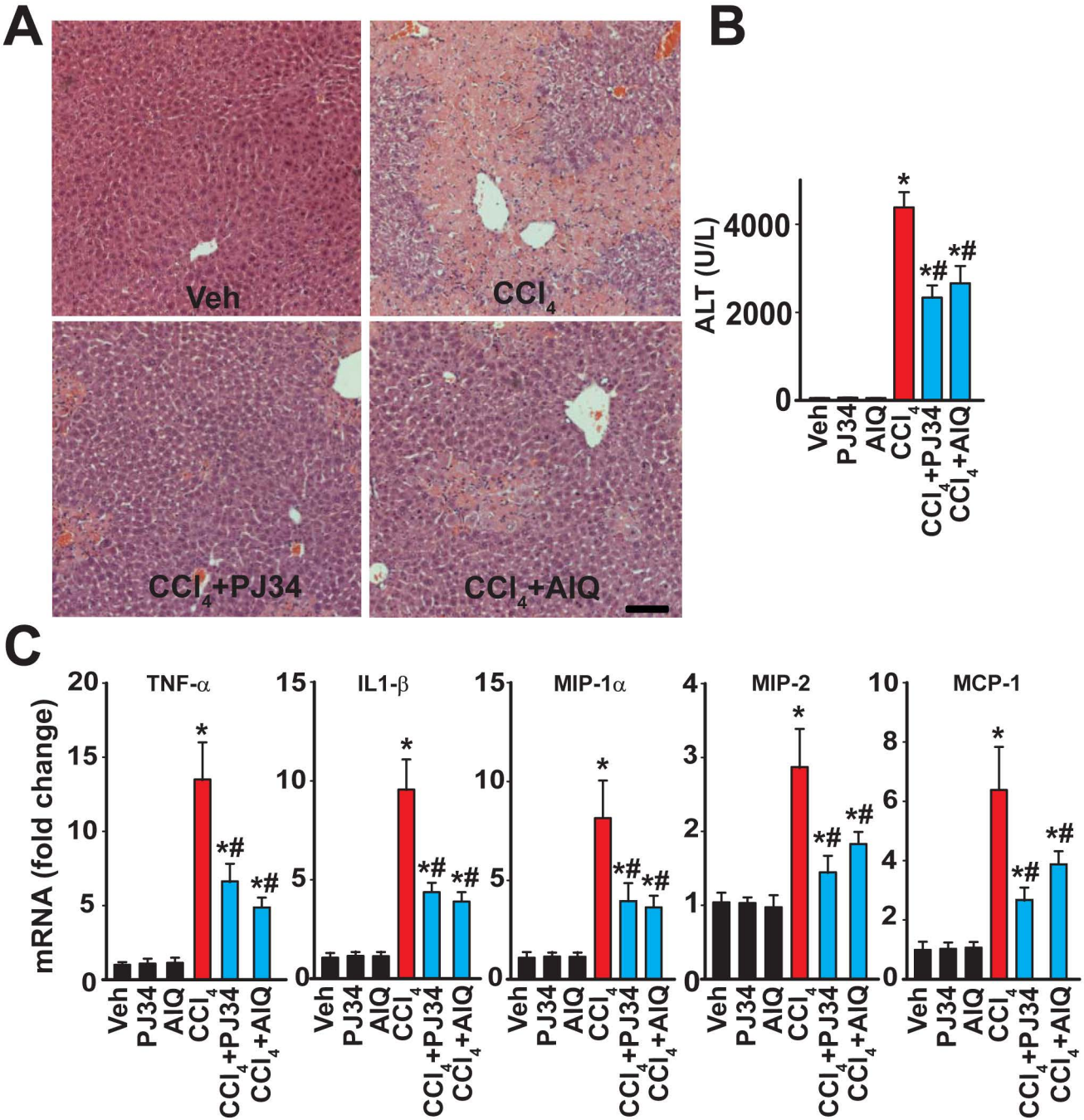
A
Veh
CCl4
CCl4+PJ34
CCl4+AIQ
B
ALT (U/L)
4000
2000
0
*
*#
*#
Veh
PJ34
AIQ
CCl4
CCl4+PJ34
CCl4+AIQ
C
mRNA (fold change)
TNF-α
IL1-β
MIP-1α
MIP-2
MCP-1
20
15
10
5
0
4
3
2
1
8
6
4
2
*
*#

Suppl. Fig. 3

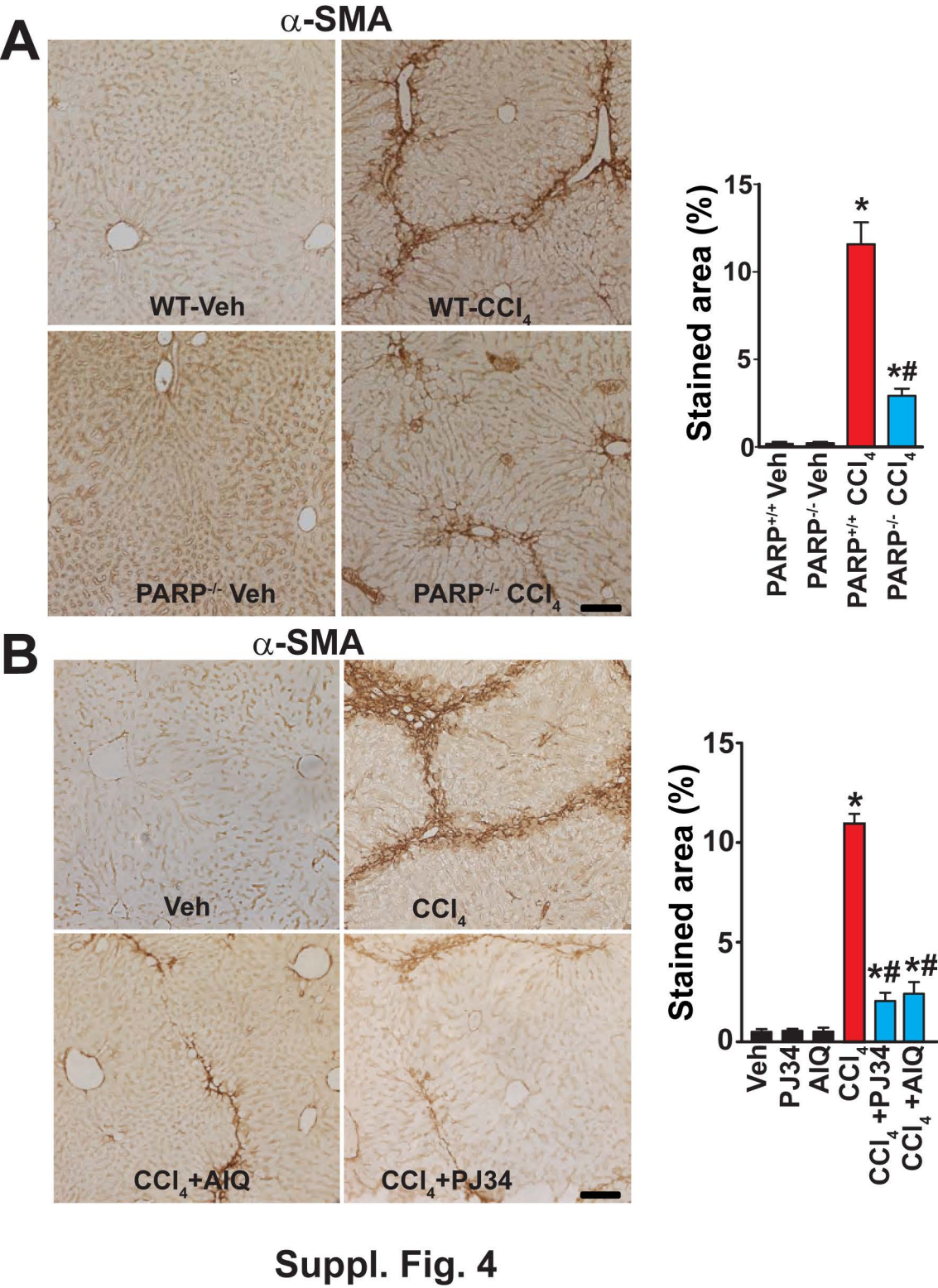
A
α-SMA
WT-Veh
WT-CCl4
PARP-/- Veh
PARP-/- CCl4
Stained area (%)
15
10
5
0
*
*#
PARP+/+ Veh
PARP-/- Veh
PARP+/+ CCl4
PARP-/- CCl4
B
α-SMA
Veh
CCl4
CCl4+AIQ
CCl4+PJ34
Stained area (%)
15
10
5
0
*
*#
*#
Veh
PJ34
AIQ
CCl4
CCl4 +PJ34
CCl4 +AIQ

Suppl. Fig. 4

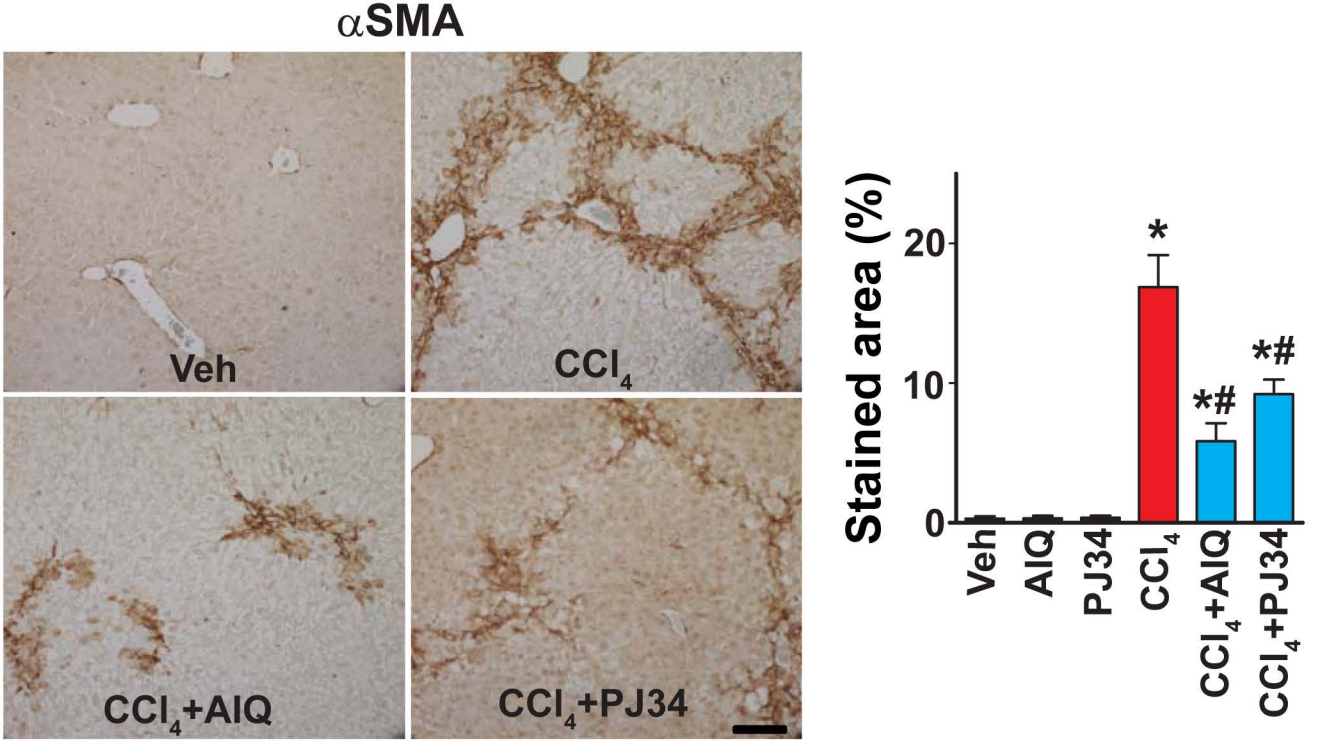
αSMA
Veh
CCl4
CCl4+AIQ
CCl4+PJ34
Stained area (%)
0
10
20
*
*#
*#
Veh
AIQ
PJ34
CCl4
CCl4+AIQ
CCl4+PJ34

Suppl. Fig. 5

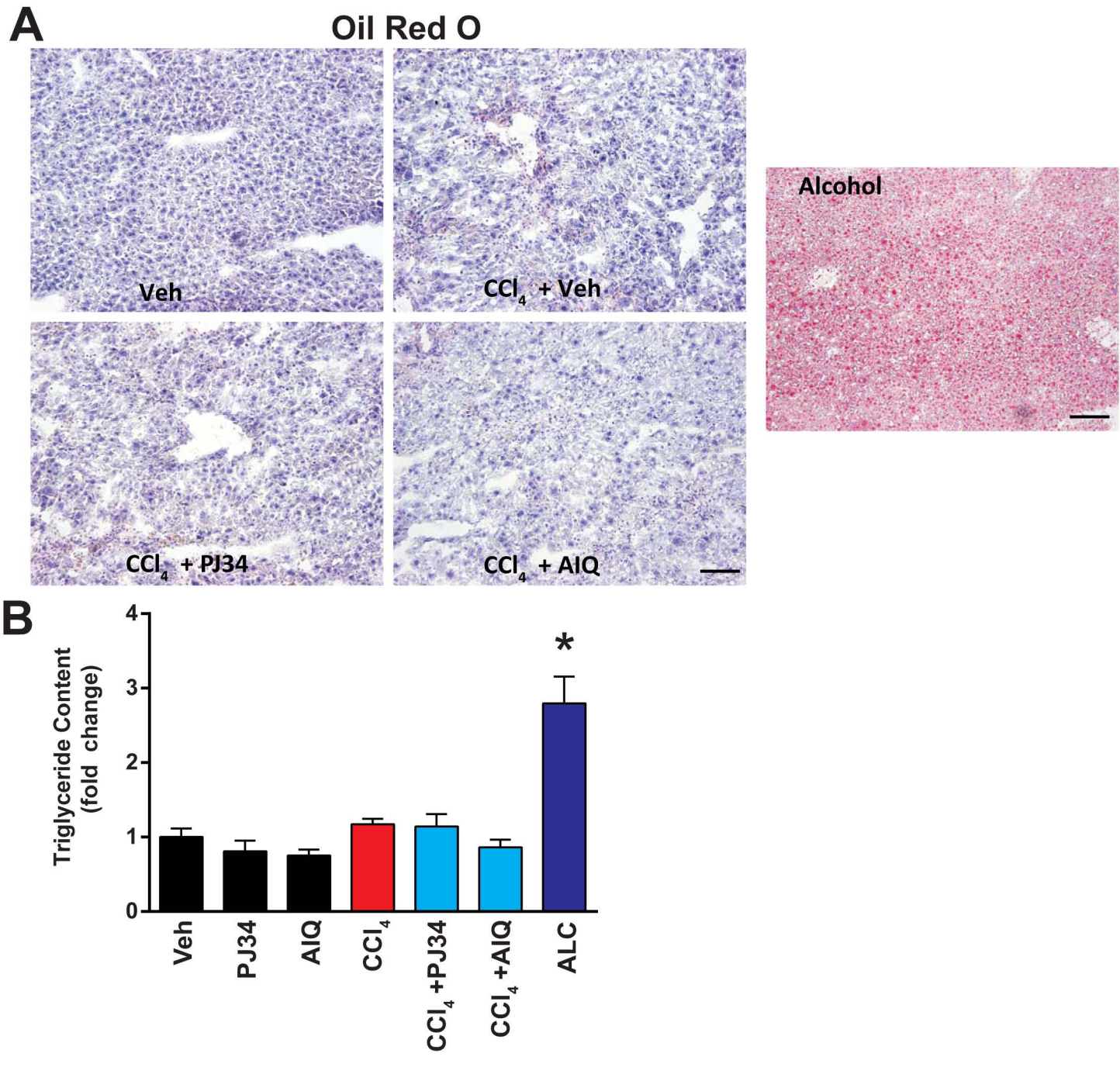
A
Oil Red O
Veh
CCl4 + Veh
CCl4 + PJ34
CCl4 + AIQ
Alcohol
B
Triglyceride Content
(fold change)
0
1
2
3
4
*
Veh
PJ34
AIQ
CCl4
CCl4 +PJ34
CCl4 +AIQ
ALC

Suppl. Fig. 6

Table S1:- List of primers and their sequences used in this study.

Gene	Forward primer	Reverse primer
TNF -α	TCTCATTCCTGCTTGTGGCAG	TCCACTTGGTGGTTTGCTACG
IL-1β	AAAAAAGCCTCGTGCTGTCG	GTCGTTGCTTGGTTCTCCTTG
MIP-1α	TGCCCTTGCTGTTCTTCTCTG	CAACGATGAATTGGCGTGG
MIP-2	AGTGAACTGCGCTGTCAATGC	AGGCAAACTTTTTGACCGCC
MCP-1	TCAGCCAGATGCAGTTAACGC	TCTGGACCCATTCCTTCTTGG
α-SMA	CTGACAGAGGCACCACTGAA	CATCTCCAGAGTCCAGCACA
TGF-b	TCTACAACCAACACAACCCGG	GAGCGCACAATCATGTTGGAC
Fibronecti	TGCAGTGACCAACATTGATCGC	AAAAGCTCCCGGATTCCATCC
CTGF	ACTATGATGCGAGCCAACTGC	TGTCCGGATGCACTTTTTGC
Collagen1	TGGCCTTGGAGGAAACTTTG	CTTGGAAACCTTGTGGACCAG
Ndufa2	GCACACATTTCCCCACACTG	CCCAACCTGCCCATTCTGAT
Ndufb3	TACCACAAACGCAGCAAACC	AAGGGACGCCATTAGAAACG
COX17	CGTGATGCGTGCATCATTGA	CATTCACAAAGTAGGCCACC
ATP5g1	GCTGCTTGAGAGATGGGTTC	AGTTGGTGTGGCTGGATCA
UCP1	GGCCCTTGTAAACAACAAAATAC	GGCAACAAGAGCTGACAGTAAAT
UCP3	ACTCCAGCGTCGCCATCAGGATTCT	TAAACAGGTGAGACTCCAGCAACTT
MCAD	GATCGCAATGGGTGCTTTTGATAGA	AGCTGATTGGCAATGTCTCCAGCAAA
ACO	CCCAACTGTGACTTCCATT	GGCATGTAACCCGTAGCACT
ACC1	GACAGACTGATCGCAGAGAAAG	TGGAGAGCCCCACACACA
ACC2	CCCAGCCGAGTTTGTCACT	GGCGATGAGCACCTTCTCTA
GK	ACATTGTGCGCCGTGCCTGTGAA	AGCCTGCGCACACTGGCGTGAAA
G6Pase	CCGGATCTACCTTGCTGCTCACTTT	TAGCAGGTAGAATCCAAGCGCGAAAC
PEPCK	CCACAGCTGCTGCAGAACA	GAAGGGTCGCATGGCAAA
mtDNA specific	CCGCAAGGGAAAGATGAAAGAC	TCGTTTGGTTTCGGGGTTTC
nuclear specific	GCCAGCCTCTCCTGATTTTAGTGT	GGGAACACAAAAGACCTCTTCTGG
b-actin	TGCACCACCAACTGCTTAG	GGATGCAGGGATGATGTTC

Table S2: Detailed information of the genes analyzed by Real-time PCR

Gene	**Full name**	**Mouse Genome Database ID**
TNF -α	tumor necrosis factor-alpha	MGI:104798
IL-1β	interleukin 1 beta	MGI:96543
MIP-1α	macrophage inflammatory protein-1alpha (also known as chemokine (C-C motif) ligand 3)	MGI:98260
MIP-2	chemokine (C-X-C motif) ligand 2	MGI:1340094
MCP-1	monocyte chemoattractant protein-1 (chemokine (C-C motif) ligand 2)	MGI:98259
α-SMA	actin, alpha 2, smooth muscle	MGI:87909
TGF-b	transforming growth factor, beta	MGI:98725
Fibronectin	fibronectin 1	MGI:95566
CTGF	connective tissue growth factor	MGI:95537
Collagen1	collagen, type I	MGI:88467
Ndufa2	NADH dehydrogenase (ubiquinone) 1 alpha subcomplex, 2	MGI:1343103
Ndufb3	NADH dehydrogenase (ubiquinone) 1 beta subcomplex 3	MGI:1913745
COX17	cytochrome c oxidase assembly protein 17	MGI:1333806
ATP5g1	ATP synthase, H+ transporting, mitochondrial F0 complex, subunit c1	MGI:107653
UCP1	uncoupling protein 1 (mitochondrial, proton carrier)	MGI:98894
UCP3	uncoupling protein 3 (mitochondrial, proton carrier)	MGI:1099787
MCAD	acyl-Coenzyme A dehydrogenase, medium chain	MGI:87867
ACO	Acyl-CoA oxidase	MGI:1330812
ACC1	acetyl-CoA carboxylase 1	MGI:108451
ACC2	acetyl-CoA carboxylase 2	MGI:2140940
GK	glucokinase	MGI:1270854
G6Pase	glucose-6-phosphatase	MGI:95607
PEPCK	phosphoenolpyruvate carboxykinase	MGI:1860456
b-actin	actin, beta	MGI:87904